RSC Advances

PAPER

View Article Online
View Journal | View Issue

Cite this: *RSC Adv.*, 2019, **9**, 24519

A room temperature operated ammonia gas sensor based on Ag-decorated TiO_2 quantum dot clusters

Haixin Liu, Wenhao Shen* and Xiaoquan Chen

In this research, nanometer size aggregates (clusters) of titanium dioxide (TiO_2) quantum dot clusters (QDs) have been successfully prepared *via* a convenient hydrolysis method at a low temperature (80 °C). Then different amounts (0–5%) of Ag were further decorated on the TiO_2 QDs *via* dipping and annealing under a nitrogen atmosphere. After Ag decoration, the TiO_2 QD sensing materials were synthesized, and characterization and NH_3 gas sensing performance studies were carried out. Analysis *via* XRD and EDS was conducted, and the results showed that Ag^+ ions were successfully reduced to Ag and decorated on the surface of the anatase TiO_2 QDs. Noble metal Ag acted as the sites for adsorbates, catalysts, or promoters during the surface reactions, and as the element improving the thermal stability of the nanostructure. Therefore, the Ag-decorated gas sensor possessed better gas sensing performance than an undecorated gas sensor, and 3% Ag dopant proved to be the optimal amount of addition. The fabricated 3% Ag-decorated TiO_2 QDs gas sensor, compared with the undecorated TiO_2 QDs sensor, displayed a 6-times-higher sensing response at room temperature and demonstrated excellent gas sensing properties toward 10–100 ppm NH_3 gas, good selectivity, gas sensitivity and stability, rapid response/recovery time, and a linear relationship between the response and the target gas concentration. In particular, the excellent performance of the Ag decorated-TiO_2 QDs gas sensor was achieved at room temperature, which suggests the great possibility of a prompt gas sensing response, with the use of paper as a substrate, that requires a low operation temperature.

Received 16th July 2019
Accepted 23rd July 2019

DOI: 10.1039/c9ra05439a

rsc.li/rsc-advances

Introduction

Recently there has been huge demand for monitoring and controlling air pollutants, of which ammonia (NH_3) is one of the most common examples that causes severe environmental problems. When ammonia is present in ecosystems in excess, it can cause nutrient imbalances and eutrophication. In terrestrial ecosystems this leads to a loss of plant species and habitat diversity, and in aquatic ecosystems this causes algal blooms and hypoxia.[1] In recent years, research into new and more effective NH_3 gas sensors using nanostructured materials has gained plenty of attention, due to the various applications, including in environmental monitoring,[2] industrial process monitoring,[3] automotive exhaust detection,[4,5] and medical diagnostics.[6,7]

One of the most commonly applied gas sensing mechanisms for NH_3 is based on resistive sensors with various metal oxide semiconductors,[2,3] such as TiO_2, ZnO,[8,9] WO_3,[10] In_2O_3,[11,12] ZrO_2,[13] V_2O_5,[14] carbon nanotubes,[15,16] Fe_2O_3 (ref. 17) and Co_3O_4.[18] In our previous work, TiO_2 QDs were successfully synthesized at a low temperature (80 °C), and their application in NH_3 gas sensors was studied. The fabricated TiO_2 QDs showed a highly porous structure and a large specific surface area, which enhanced their gas sensing performance toward NH_3 at room temperature. A comparison with other reported NH_3 gas sensors is shown in Table 1. These previous reports imply that NH_3 gas sensors prepared using nanomaterials have the disadvantages of requiring high temperatures, demonstrating low sensitivity and involving complex synthesis processes. In order to solve these problems, much effort has been devoted to this area with attempts to control the particle size and morphology,[19] maximize the exposure of active crystal facets,[20,21] introduce transition metal dopants,[22,23] metal oxide additives[24] or noble metal sensitizers,[19,24,25] and make composites with conducting polymers. It has been proven that nanoparticles of noble metals (Pd, Rh, Pt, Au, Ag) on the surface of metal oxides can act as the sites for adsorbates, catalysts, or promoters during surface reactions and as the element that improves the thermal stability of the film nanostructure.[23,26,27] Of these, the low price of Ag dopants compared to other noble metals is beneficial for their practical application; moreover, as reported, the gas sensing properties of various kinds of semiconductors are promoted markedly by Ag dopants.[28] Furthermore, with the aim of printing sensing materials on paper substrates to fabricate wearable and flexible gas sensors, to further enhance the gas sensing performance at room temperature, the testing of curved substrates is needed. Therefore, Ag-decorated TiO_2 QD sensing materials were prepared, and their

State Key Laboratory of Pulp and Paper Engineering, South China University of Technology, Guangzhou, 510640, P. R. China. E-mail: ppwhshen@scut.edu.cn

Table 1 Comparisons of the sensor responses to NH_3 with different sensing materials

No.	Material	Concentration (ppm)	Response ($R = R_a/R_g$)	Temperature (°C)	Ref.
1	WO_3	300	2.39	250	29
2	V_2O_5	1	11.3	200	14
3	Pd–ZnO	5	7.1	210	30
4	TiO_2 QDs	10	7.8	RT	Our previous work[31]
5	SnO_2/MWCNTs	100	12.5	RT	26
6	PANI/TiO_2	23	1.7	RT	32
7	TiO_2/PPy	30	3.52	RT	33
8	PANI–TiO_2	20	12.5	RT	34
9	Ag–TiO_2 QDs	20	25.1	RT	Present work

gas sensing performance was promoted with an alumina tube as the substrate. With different thicknesses and sizes of the prepared sensor, the resistance was different, so the baseline was different to our previous work; but compared with TiO_2 QDs sensors on an alumina tube, the Ag–TiO_2 QDs gas sensor still showed better performance.

In this context, this paper is focused on the fabrication of a NH_3 sensor based on Ag-decorated TiO_2 QDs *via* a facile annealing route to enhance the NH_3 sensing performance at room temperature. To the best of our knowledge, an Ag-decorated TiO_2 QDs NH_3 gas sensor has not yet been reported in the literature. The fabricated sensors were evaluated systematically in terms of their response, response/recovery times and selectivity toward NH_3. The main target of this work is to promote the gas sensing performance toward NH_3 at room temperature on a curved substrate (alumina tube). The fabricated Ag-decorated TiO_2 QDs gas sensor successfully showed a response several times higher than that of an undecorated gas sensor.

Experimental

Synthesis of anatase TiO_2 QDs

The TiO_2 QDs were prepared according to a previous work,[31] and the detailed synthesis process is as follows. (1) Tetrabutyl titanate ($Ti(OC_4H_9)_4$, 10 mL) and acetic anhydride ($(CH_3CO)_2O$, 20 mL) were mixed with cyclohexane (50 mL) in a glass vessel with a screw-on cap. The mixture was then heated to 80 °C until it appeared turbid. After maintaining the reaction for 30 min, the solid product was centrifuged from the reaction mixture, washed several times with acetone and distilled water, and dried to provide the titanyl organic compound. (2) The titanyl organic compound was mixed with water ($H_2O : TiO_2 = 50 : 1$ mol mol^{-1}), and then nitric acid (HNO_3) solution was added at a concentration of 1 mol L^{-1}. The mixture was then heated and continuously stirred at 60 °C for 3 h to obtain the TiO_2 QDs. The prepared TiO_2 QDs were settled through controlling the pH and collected *via* centrifugation. After washing with ethanol and DI water several times and drying at 60 °C overnight, TiO_2 QD powder was acquired.

Synthesis of Ag-decorated TiO_2 QDs

The obtained TiO_2 QDs were then divided into five equal portions and mixed with distilled water. Different amounts of $AgNO_3$ were added to the five mixtures, respectively. The molar ratio of Ag/Ti was set at 0%, 1%, 3% or 5%, individually. Subsequently, the mixtures were ultrasonically agitated for 15 min until they were homogeneous. Then the mixtures were annealed under a nitrogen atmosphere *via* two steps: step 1 was to dry the material at 80 °C for 6 h, followed by a temperature of 550 °C for 4 h (step 2) to obtain the Ag-decorated TiO_2 QDs gas sensing materials.

Characterization

Before the investigations into the gas sensing performance of the gas sensors, the gas sensing materials were characterized *via* XRD, SEM, EDS, TEM and BET analysis methods. The crystalline structure and phase composition were characterized using an X-ray diffractometer (XRD, Bruker, Germany), with Cu Kα radiation at a wavelength of 1.5406 Å, operating at 40 kV and 30 mA. The morphology was observed using a scanning electron microscope (SEM, Merlin, Germany) with an operation voltage of 5 kV. A transmission electron microscope (TEM, JEM-2200FS, Japan) was used to further characterize the crystallographic features. The gas sensing performance of the sensor was evaluated using a WS-30A gas sensor measurement system (Weishen Electronic Technology Co., Ltd, China).

Gas sensor fabrication and measurements

The fabrication process of the gas sensor was as follows: (1) the as-prepared gas sensing material was mixed with absolute ethyl alcohol at a weight ratio of 4 : 1 and the mixed solution was ultrasonically agitated for 15 min until a homogeneous slurry was formed; (2) the slurry was pasted onto an alumina tube that had a pair of Au electrodes and four Pt wires for resistance measurements; and (3) the alumina tube was annealed at 300 °C for 2 h to improve the stability of the sensor and remove residual organics on the surface of the sensor.

As shown in Fig. 1a, the structure of the gas sensor is explained as follows: a pair of gold electrodes connected to Pt wires is printed on the alumina tube, and the area between the two gold electrodes is coated with the as-prepared gas sensing material. Fig. 1b displays the circuit used to measure the gas sensor, where R_f is a load resistor connected in series with the gas sensor and R_S donates the resistance of the sensor. In the testing process, an appropriate bias voltage ($V_{working} = 5$ V) was applied. The response of the sensor was measured by

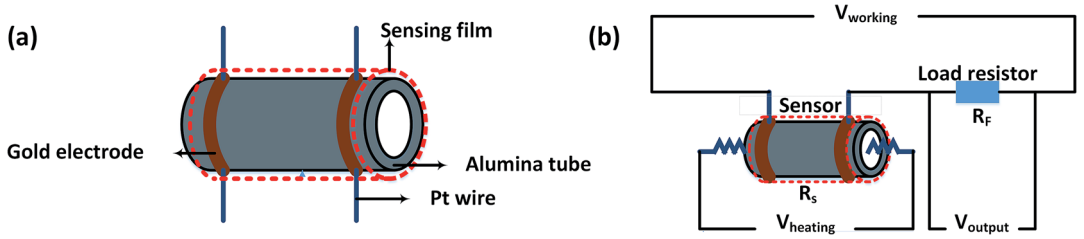

Fig. 1 (a) A schematic diagram of the gas sensor and (b) the electric circuit used to investigate the gas sensor.

monitoring the voltage (V_{output}) changes of R_F. The gas response (S) of the sensor is defined as $S = R_a/R_g$ for reducing gases and $S = R_g/R_a$ for oxidizing gases, where R_g and R_a are the resistance values of the sensor measured in the target gas and in air, respectively.

The experimental setup for the gas sensing measurement system is shown in Fig. 2. The fabricated sensor was set-up on a testing board in an 18 L testing chamber that was connected to the gas sensing measurement system. The temperature and humidity of the chamber were maintained at 25 °C and 50%, respectively. The concentrations of the testing gases (NH_3, C_2H_5OH, CH_2O, C_6H_6 and H_2S) mixed with air were controlled *via* two mass flow controllers.

Results and discussion

Structural and morphological characteristics

Before any investigation of the gas sensing performance, the Ag-decorated TiO_2 QDs were characterized with XRD, SEM and EDS technologies. The results are addressed below.

XRD was conducted to investigate the crystal structures of the as-synthesized samples. The results of measurements are shown in Fig. 3. In the case of the TiO_2 QDs, the pattern was in accordance with anatase TiO_2 reflections (JCPDS no. 04-0477), and all the diffraction peaks correspond well to the (101), (004), (200), (105), (211), (204), (220), and (215) peaks of anatase TiO_2. Compared with the TiO_2 QDs, all the patterns of the Ag-decorated TiO_2 QDs sensing materials revealed the presence of the diffraction peaks of anatase TiO_2 along with additional peaks at $2\theta = 38.1°$, 44.3°, 64.4° and 77.4°, which corresponded well with the (111), (200), (220) and (311) peaks of spinel silver (JCPDS no. 65-2871). In addition, the intensities increase when the concentration of Ag dopant is higher. Moreover, these anatase TiO_2 and spinel diffraction peaks were present in all the Ag-decorated samples without any shifts, indicating that the metal dopants were merely placed on the surfaces of the crystals rather than being covalently anchored into the crystal lattices.[28] Compared to our previous work, at higher annealing temperatures, the crystallinity is higher and small rutile TiO_2 peaks were also observed in all the samples, where the appearance of rutile TiO_2 diffraction peaks was due to phase transformation from anatase TiO_2 to rutile TiO_2 at high annealing temperatures (550 °C).[35] In addition, from eqn (1), the calculated crystallite size of the TiO_2 QDs was 66 nm, and the average crystallite sizes of the 1%, 3% and 5% Ag-decorated TiO_2 QDs sensing materials were 31.2, 30.8, and 34.2 nm, respectively.

$$D = \frac{K\lambda}{B\cos\theta} \quad (1)$$

where K is the Scherrer constant (equal to 0.89), B is the full width at half maximum (FWHM) of the diffraction peak, θ is the diffraction angle, λ is the wavelength of the X-rays, and D is the crystal size.

SEM, TEM and EDS technologies were utilized to characterize the TiO_2 QDs and Ag-decorated sensing materials. TEM

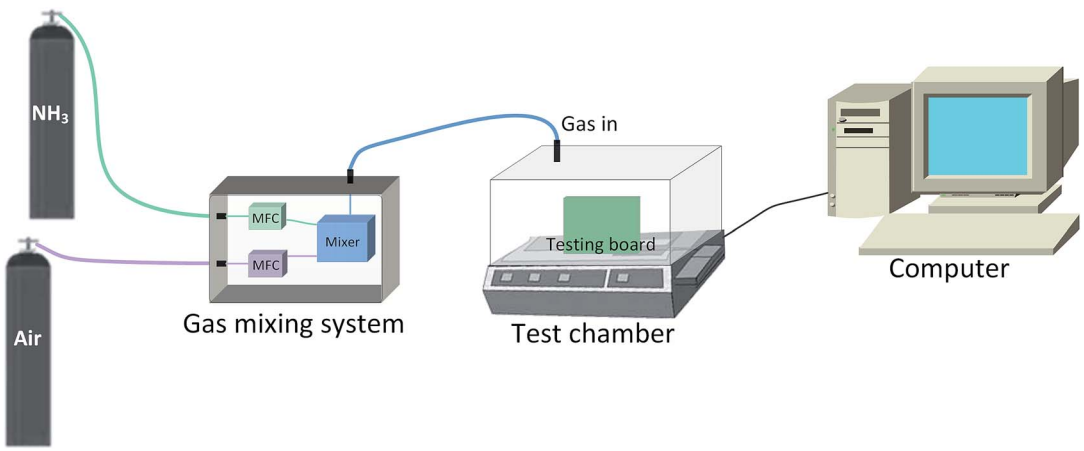

Fig. 2 The experimental setup for gas sensing measurements.

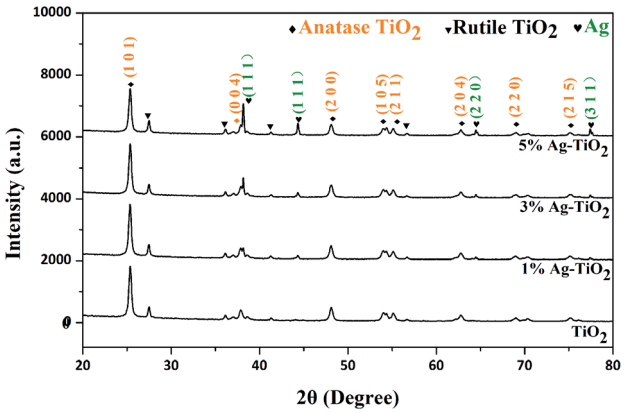

Fig. 3 The XRD patterns of the TiO_2 QDs and the Ag-decorated TiO_2 QDs sensing materials.

images of the TiO_2 QDs are shown in Fig. 4a and b; as we can see, the synthesized stable nanometer size aggregates with good dispersibility were TiO_2 quantum dot clusters with a uniform size of 66 nm, they were formed from 2–5 nm diameter anatase crystals. Similar to our reported work,[31] with a unique formation method, the TiO_2 QDs show a highly porous structure (Fig. 4b) with a huge specific surface area of 315.74 $m^2\ g^{-1}$.[31] In our previous work, the sensor was fabricated on a flat substrate; for further research, to achieve fabrication on a paper substrate for a flexible sensor, we need to test it on a curved substrate and then we can start optimizing the sensing material on a tubular substrate to achieve better sensing performance at room temperature. Our coming work is aimed at compositing the nanoparticles with two-dimensional GO to achieve flexible sensors on paper to simplify the fabrication process with printing technology. After considering the noble metal Ag as the catalyst, Ag-decorated TiO_2 QDs were synthesized. Following coating on an alumina tube, the SEM results are displayed in Fig. 4c. The film is densified and porous between the grains of the film, which is an advantage for the diffusion of the target gas. However, the decorated Ag cannot be seen in the film, maybe due to its low concentration or small size. Then, EDS analysis was introduced; the elemental mapping images of the Ag-decorated TiO_2 sensing material are displayed in Fig. 4d–i, where all scale bars are 10 μm. Fig. 4d shows an SEM image, and Fig. 4f–i clearly highlight the presence of C, Ti, O, and Ag elements. It is notable that the good dispersion of the Ag dopant is revealed in Fig. 4i; the detected C elements in Fig. 4f are attributed to the conducting resin that was applied during the preparation of the sample for SEM characterization. The XRD (Fig. 3) and EDS (Fig. 4) characterization results indicate that the Ag dopant was successfully decorated on the surface of the TiO_2 sensing material.

Gas sensing properties and mechanism

To further enhance the gas sensing properties, the dopant Ag was added to form Ag-decorated QDs sensing materials, and

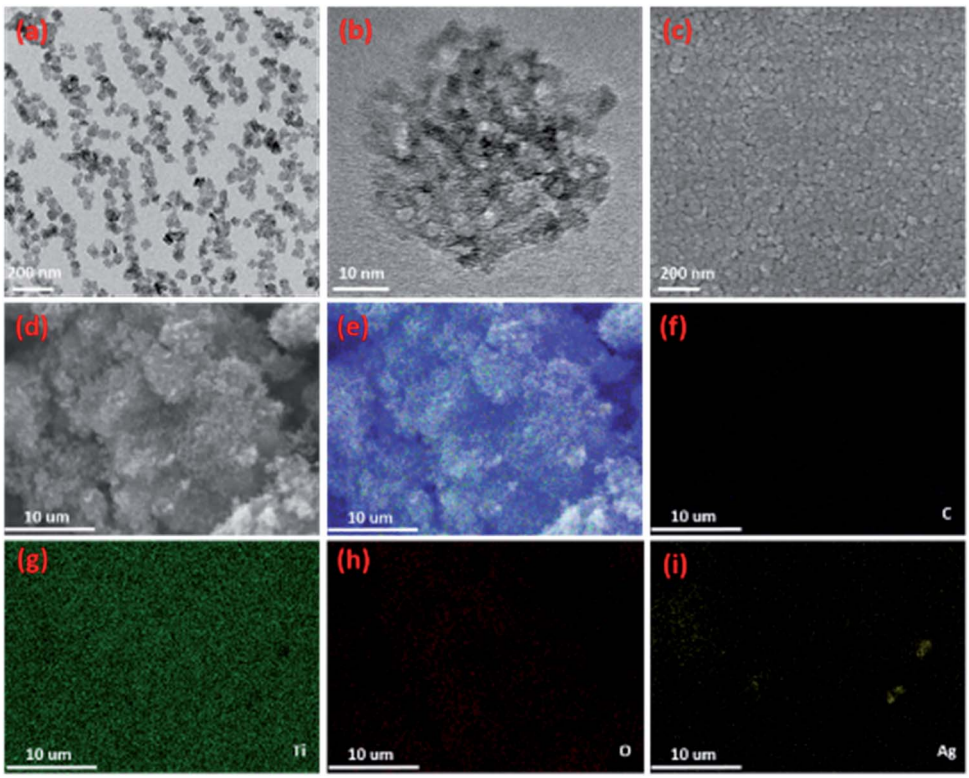

Fig. 4 TEM images of (a) TiO_2 QDs and (b) a single nanoparticle. An SEM image of (c) Ag-decorated TiO_2 QDs film. The EDS results from an Ag-decorated TiO_2 sensing material sample: (d) SEM image; (e) overall mapping; and (f–i) EDS elemental mapping images of C, Ti, O and Ag.

corresponding Ag-decorated TiO_2 QDs gas sensors were developed and tested.

Optimal amount of Ag dopant addition

After having decorated the material with the dopant Ag at 0%, 1%, 3% and 5%, respectively, different Ag-decorated TiO_2 QDs gas sensors were fabricated and exposed to 20, 40, 60, and 80 ppm NH_3 gas, successively, and the gas sensing performances were measured and are given in Fig. 5. Compared with the undecorated TiO_2 QDs gas sensor, all Ag-decorated TiO_2 QDs gas sensors displayed higher responses (Fig. 5a) and shorter response/recovery times (Fig. 5b, c and Table 2). In the results shown in Fig. 5, the 3% Ag-decorated TiO_2 QDs gas sensor possessed the best gas sensing performance; its sensing response and response/recovery time were 6 times higher and shorter, respectively, than those of the pure TiO_2 QDs gas sensor, which meets our goal and will benefit our future research. Therefore, all subsequent experiments were carried out with the 3% Ag-decorated TiO_2 QDs sensor.

From the results in Fig. 5, it is evident that the noble metal Ag greatly improves the gas sensing behaviour of the sensor upon exposure to NH_3 gas. Moreover, the abrupt decrease in the response of the sensor decorated with higher amounts of Ag than the optimal 3% (Fig. 5a) was probably due to a reduction in the number of active sites (Ag particles), which was correlated with the agglomeration of Ag grains.[36,37] As for the mechanism of the performance enhancement with the Ag dopant, it could be attributed to the following factors. (1) The decorated noble metal Ag not only provides specific adsorption sites in the form of single particles mixed in the matrix, but most Ag elements can often act as catalysts. Thus, the contact potential barrier of the material is decreased and the interfacial effect is enhanced, and therefore the sensing reaction is promoted.[38] Generally, a chemiresistive semiconductor sensor is based on the resistance of the sensing material changing due to chemical and electronic interactions between the adsorbed gas and the sensing material. The sensing mechanism can be described in terms of an oxygen adsorption reaction on the sensing material surface, which strongly depends on the operating temperature; the stable oxygen ions are O_2^-, O^- and O^{2-}, which operate below 100 °C, from 100–300 °C, and above 300 °C, respectively.[39] Hence, the oxygen adsorption reactions can be represented as follows:

$$O_2\ (gas) \rightarrow O_2\ (ads) \quad (2)$$

$$O_2\ (ads) + e^- \rightarrow O_2^-\ (ads) \quad (3)$$

$$2NH_3 + 3O_2^-\ (ads) \rightarrow 3H_2O + 3e^- \quad (4)$$

Linearity between the response and the target gas concentration

With optimal 3% Ag dopant addition, the behavior of the Ag-decorated TiO_2 QDs gas sensor towards different levels of NH_3 gas at room temperature was further investigated. After having been exposed to NH_3 gas at concentrations from 10 ppm up to 100 ppm, separately, the corresponding responses of the Ag-

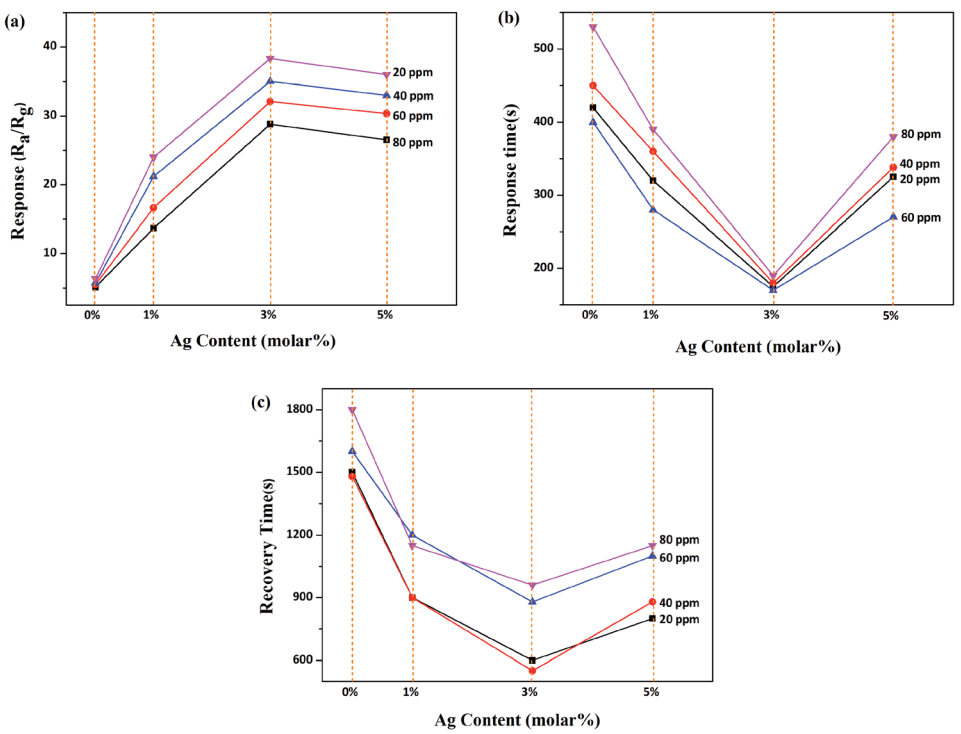

Fig. 5 A performance comparison between Ag-decorated TiO_2 QDs gas sensors with different volumes of Ag addition to NH_3: (a) response; (b) response time; and (c) recovery time.

Table 2 Comparisons of the response and recovery time of the Ag-decorated TiO_2 QDs gas sensors to NH_3 with different volume of additions

Sample	Response time (s) 20 ppm	Recovery time (s) 20 ppm	Response time (s) 40 ppm	Recovery time (s) 40 ppm	Response time (s) 60 ppm	Recovery time (s) 60 ppm	Response time (s) 80 ppm	Recovery time (s) 80 ppm
0%	420	1500	450	1480	400	1600	530	1800
1%	320	900	360	900	280	1200	390	1150
3%	175	600	180	550	170	880	190	960
5%	325	800	338	880	270	1100	380	1150

decorated TiO_2 QDs gas sensor are shown in Fig. 6. It is clearly indicated in Fig. 6a that the responses of the sensor increased with an increase in the concentration of NH_3 gas, where the sensing responses to 10 ppm and 100 ppm NH_3 gas were 25.1 and 40.7, respectively. It is noteworthy that, even at a low level of 10 ppm NH_3, this particular Ag-decorated TiO_2 QDs gas sensor still exhibited a reasonably high sensing response of 25.1. Besides, the results in Fig. 6b demonstrated good linearity between the sensing response and the NH_3 concentration, and linear equation for the correlation is $S = 0.166C_{NH_3} + 24.738$, where S is the response sensitivity and C_{NH_3} is the NH_3 concentration; the regression coefficient is 0.975. In addition, in order to calculate the limit of detection (LOD) of the sensor, the signal response (S) at different NH_3 concentrations was analyzed *via* linear regression ($y = a + bx$). The LOD $= 3\sigma_D/s \approx$ 0.217 ppm, where σ_D is the standard deviation of the y-intercept and s is the slope of the calibration curve. With all these results, a possible low detection limit at the ppb level is implied.

Response/recovery time, selectivity and stability

In addition to the above sensing response, the response/recovery time, selectivity and stability are also critical characteristics for gas sensors, and these gas sensing properties were further investigated.

Firstly, comparisons of the response/recovery time at different NH_3 gas concentrations for the Ag-decorated TiO_2 QDs gas sensor are plotted in Fig. 7a. Obviously, the sensor responded faster than it recovered generally; the response time showed a tiny variation upon exposure to different levels of NH_3 gas, whereas the recovery time became longer with an increase in NH_3 concentration (60 to 100 ppm). Secondly, in the study, the selectivity of the Ag-decorated TiO_2 QDS gas sensor was studied through exposing the sensor to 10 ppm C_2H_5OH, CH_2O, H_2S, C_6H_6 and NH_3 gases, individually. As indicated clearly in Fig. 7b, the sensor displayed no significant sensitivities to the gases C_2H_5OH, CH_2O, H_2S and C_6H_6; it conversely demonstrated a very high sensitivity to NH_3 gas, where the sensing response was almost 10 times higher than towards the other four kinds of gas. This result clearly revealed that the Ag-decorated TiO_2 QDS gas sensor had excellent selectivity for NH_3 gas. Lastly, the investigation of the long-term stability of the Ag-decorated TiO_2 QDs gas sensor was conducted *via* putting the sensor under a 10 ppm NH_3 atmosphere for 45 days. The measured results in Fig. 7c reveal that only a tiny fluctuation in the sensing response was observed during this period, which indicates that the sensor possesses a stable response to NH_3 gas.

From the above-demonstrated good linearity (Fig. 6b), rapid response/recovery time (Fig. 7a), and excellent sensitivity (Fig. 7b) and stability (Fig. 7c) performances of the developed NH_3 sensor based on the Ag-decorated TiO_2 QDs sensing material, it is particularly important to highlight that this excellent gas sensing performance was achieved at room temperature. In recent years, most reported work on NH_3 gas sensors has been conducted at high temperatures, whereas NH_3 sensors operating at room temperature have been limited. Therefore, in the present study, the excellent gas sensing performance of the developed Ag-decorated TiO_2 QDs gas sensor at room temperature suggests the following prospects: (1) since there is no need for the sensor to be heated to

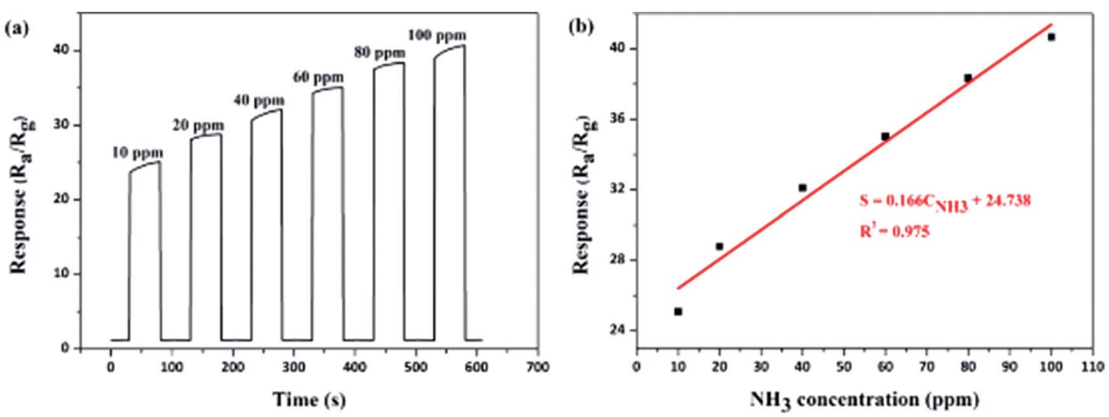

Fig. 6 Gas sensing properties of the Ag-decorated TiO_2 QDs gas sensor to different concentrations of NH_3 gas: (a) dynamic response; and (b) the correlation between the response and concentration.

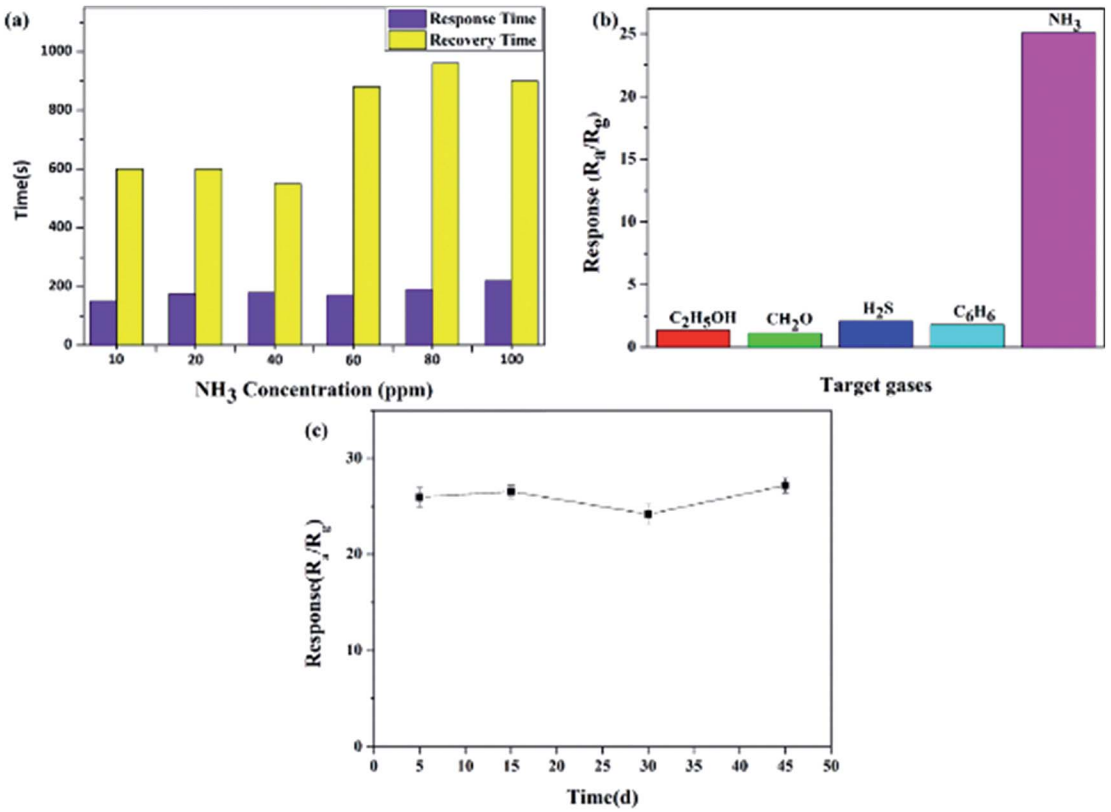

Fig. 7 The gas sensing properties of the Ag-decorated TiO_2 QDs gas sensor: (a) response/recovery time at different NH_3 gas concentrations; (b) selectivity to different gases at 10 ppm; and (c) stability towards 10 ppm NH_3.

a required temperature, as shown in Fig. 7a, this implies that a prompt response could be achieved when operating at room temperature; (2) the presented room temperature operation of the Ag-decorated TiO_2 QDs gas sensor showed a great possibility for using flexible natural green fibers as substrates in the fabrication of a gas sensor in which a low operation temperature is the key point.

Conclusions and prospects

Based on an Ag-decorated TiO_2 QDs sensing material, an NH_3 gas sensor was fabricated, and its gas sensing performance at room temperature was studied. The study results were as follows. (1) The characterization results from the Ag-decorated TiO_2 sensing material displayed that the decorated Ag was in the form of spinel silver and displayed uniform distribution. Targeting NH_3 gas and operation at room temperature, the optimal amount of Ag dopant addition was determined to be 3%, and gas sensing study results from the 3% Ag-decorated TiO_2 QDs gas sensor toward 10–100 ppm NH_3 gas revealed that the Ag-decorated TiO_2 QDs gas sensor not only possessed good NH_3 selectivity, gas sensitivity, stability and linearity, but it also showed rapid response and recovery times. Even at a low concentration of 10 ppm NH_3 gas, it still had a high response of 25.1, a rapid response time of 150 s and a recovery time of 600 s. (2) The point most worth mentioning is that the excellent gas sensing performance of the Ag-decorated TiO_2 QDs gas sensor was achieved at room temperature. This innovation showed the following great possibilities: (i) since there is no need for the sensor to be heated to a required high operating temperature, a prompt gas-sensing response can be achieved; and (ii) from a biodegradable view, a gas sensor can be developed with flexible natural green fibers as substrates in which a low operation temperature is the key point. This will be the focus of our future work.

Conflicts of interest

There are no conflicts of interest to declare.

Acknowledgements

The research was supported by the Research Funds of Joint Research for International Cooperation on Scientific and Technological Innovation by MOST (2017YFE9134900), the Science and Technology Program of Guangzhou, China (No. 201904010423), and the National Science Foundation of Guangdong Province, China (No. 2016A030313478).

Notes and references

1 R. W. Pinder, A. B. Gilliland and R. L. Dennis, *Geophys. Res. Lett.*, 2008, **35**, 82–90.

2 J. W. Erisman, R. Otjes, A. Hensen, P. Jongejan, P. van den Bulk, A. Khlystov, H. Möls and S. Slanina, *Atmos. Environ.*, 2001, **35**, 1913–1922.
3 T. D. Durbin, R. D. Wilson, J. M. Norbeck, J. W. Miller, T. Huai and S. H. Rhee, *Atmos. Environ.*, 2002, **36**, 1475–1482.
4 Y.-L. Tang, Z.-J. Li, J.-Y. Ma, Y.-J. Guo, Y.-Q. Fu and X.-T. Zu, *Sens. Actuators, B*, 2014, **201**, 114–121.
5 S.-Y. Wang, J.-Y. Ma, Z.-J. Li, H. Q. Su, N. R. Alkurd, W.-L. Zhou, L. Wang, B. Du, Y.-L. Tang, D.-Y. Ao, S.-C. Zhang, Q. K. Yu and X.-T. Zu, *J. Hazard. Mater.*, 2015, **285**, 368–374.
6 R. E. de la Hoz, D. P. Schlueter and W. N. Rom, *Am. J. Ind. Med.*, 1996, **29**, 209–214.
7 W. Ament, J. Huizenga, E. Kort, T. van der Mark, R. Grevink and G. Verkerke, *Int. J. Sports Med.*, 1999, **20**, 71–77.
8 C. Baratto, *RSC Adv.*, 2018, **8**, 32038–32043.
9 G. N. Dar, A. Umar, S. A. Zaidi, S. Baskoutas, S. W. Hwang, M. Abaker, A. Al-Hajry and S. A. Al-Sayari, *Talanta*, 2012, **89**, 155–161.
10 C. Xu, N. Miura, Y. Ishida, K. Matsuda and N. Yamazoe, *Sens. Actuators, B*, 2000, **65**, 163–165.
11 D. Han, P. Song, H. Zhang, H. Yan, Q. Xu, Z. Yang and Q. Wang, *RSC Adv.*, 2014, **4**, 50241–50248.
12 P. Guo and H. Pan, *Sens. Actuators, B*, 2006, **114**, 762–767.
13 A. Satsuma, K. Shimizu, T. Hattori, H. Nishiyama, S. Kakimoto, S. Sugaya and H. Yokoi, *Sens. Actuators, B*, 2007, **123**, 757–762.
14 V. Modafferi, G. Panzera, A. Donato, P. L. Antonucci, C. Cannilla, N. Donato, D. Spadaro and G. Neri, *Sens. Actuators, B*, 2012, **163**, 61–68.
15 J. Huang, J. Wang, C. Gu, K. Yu, F. Meng and J. Liu, *Sens. Actuators, A*, 2009, **150**, 218–223.
16 E. Bekyarova, M. Davis, T. Burch, M. E. Itkis, B. Zhao, S. Sunshine and R. C. Haddon, *J. Phys. Chem. B*, 2004, **108**, 19717–19720.
17 W. Kim, J. S. Lee and J. Jang, *RSC Adv.*, 2018, **8**, 31874–31880.
18 J. Deng, R. Zhang, L. Wang, Z. Lou and T. Zhang, *Sens. Actuators, B*, 2015, **209**, 449–455.
19 Z. Jing and J. Zhan, *Adv. Mater.*, 2008, **20**, 4547–4551.
20 S. Tian, F. Yang, D. Zeng and C. Xie, *J. Phys. Chem. C*, 2012, **116**, 10586–10591.
21 K. Anand, O. Singh, M. P. Singh, J. Kaur and R. C. Singh, *Sens. Actuators, B*, 2014, **195**, 409–415.
22 D. Xue, R. Zhou, X. Lin, X. Duan, Q. Li and T. Wang, *RSC Adv.*, 2019, **9**, 4150–4156.
23 J. Haeng Yu and G. Man Choi, *Sens. Actuators, B*, 1998, **52**, 251–256.
24 H. Gong, J. Q. Hu, J. H. Wang, C. H. Ong and F. R. Zhu, *Sens. Actuators, B*, 2006, **115**, 247–251.
25 I. P. Liu, C. H. Chang, T. C. Chou and K. W. Lin, *Sens. Actuators, B*, 2019, **291**, 148–154.
26 V. Srivastava and K. Jain, *Sens. Actuators, B*, 2008, **133**, 46–52.
27 C. Cannilla, G. Bonura, F. Frusteri, D. Spadaro, S. Trocino and G. Neri, *J. Mater. Chem. C*, 2014, **2**, 5778.
28 Y. Tang, Z. Li, X. Zu, J. Ma, L. Wang, J. Yang, B. Du and Q. Yu, *J. Hazard. Mater.*, 2015, **298**, 154–161.
29 N. Van Hieu, V. Van Quang, N. D. Hoa and D. Kim, *Curr. Appl. Phys.*, 2011, **11**, 657–661.
30 Y. Zeng, Z. Lou, L. Wang, B. Zou, T. Zhang, W. Zheng and G. Zou, *Sens. Actuators, B*, 2011, **156**, 395–400.
31 H. Liu, W. Shen, X. Chen and J. P. Corriou, *J. Mater. Sci.: Mater. Electron.*, 2018, **29**, 18380–18387.
32 H. Tai, Y. Jiang, G. Xie, J. Yu, X. Chen and Z. Ying, *Sens. Actuators, B*, 2008, **129**, 319–326.
33 H. Tai, Y. Jiang, G. Xie, J. Yu and M. Zhao, *Int. J. Environ. Anal. Chem.*, 2007, **87**, 539–551.
34 J. Gong, Y. Li, Z. Hu, Z. Zhou and Y. Deng, *J. Phys. Chem. C*, 2010, **114**, 9970–9974.
35 C.-L. Wang, W.-S. Hwang, H.-L. Chu, H.-J. Lin, H.-H. Ko and M.-C. Wang, *Ceram. Int.*, 2016, **42**, 13136–13143.
36 S. Pandey and K. K. Nanda, *ACS Sens.*, 2016, **1**, 55–62.
37 G. Xu, Y. W. Zhang, X. Sun, C. L. Xu and C. H. Yan, *J. Phys. Chem. B*, 2005, **109**, 3269–3278.
38 L. Chen and S. C. Tsang, *Sens. Actuators, B*, 2003, **89**, 68–75.
39 M. Takata, D. Tsubone and H. Yanagida, *J. Am. Ceram. Soc.*, 1976, **59**, 4–8.